Available online at www.eccomasproceedia.org
Eccomas Proceedia COMPDYN (2019) 1907-1923

ECCOMAS
Proceedia

COMPDYN 2019
7th ECCOMAS Thematic Conference on
Computational Methods in Structural Dynamics and Earthquake Engineering
M. Papadrakakis, M. Fragiadakis (eds.)
Crete, Greece, 24–26 June 2019

COMPARATIVE ASSESSMENT OF DYNAMIC SOIL-STRUCTURE INTERACTION MODELS FOR FRAGILITY CHARACTERISATION

Francesco Cavalieri[1], António A. Correia[2], Helen Crowley[3], and Rui Pinho[4,5]

[1] European Centre for Training and Research in Earthquake Engineering (EUCENTRE)
Via Adolfo Ferrata 1, 27100 Pavia, Italy
e-mail: francesco.cavalieri@eucentre.it

[2] Laboratório Nacional de Engenharia Civil (LNEC)
Av. do Brasil 101, 1700-066 Lisboa, Portugal
e-mail: aacorreia@lnec.pt

[3] Seismic Risk Consultant
27100 Pavia, Italy
e-mail: helen.crowley78@gmail.com

[4,5] University of Pavia, via Adolfo Ferrata 5, 27100 Pavia, Italy
Mosayk Ltd., via Fratelli Cuzio 42, 27100 Pavia, Italy
e-mail: rui.pinho@unipv.it, rui.pinho@mosayk.it

Abstract

Dynamic soil–structure interaction (SSI), involving the coupling of structure, foundation and soil, is a crucial and challenging problem, especially when soil nonlinearity plays an important role. This paper shows the impact of adopting different SSI models on the assessment of seismic fragility functions. The substructure approach is initially adopted by implementing two models, the first of which includes only a translational elastic spring and a dashpot. The second and more refined model is a Lumped-Parameter Model (LPM) accounting for frequency dependence of the impedance. An additional approach including soil nonlinearities is also employed. A nonlinear macro-element is introduced to model the near-field behaviour by condensing the entire soil-foundation system into a single nonlinear element at the base of the superstructure. Energy dissipation through radiation damping is also accounted for. The comparison between the adopted approaches is evaluated in terms of their effects on the characterisation of fragility functions for unreinforced masonry buildings.

Keywords: Induced seismicity, Lumped-Parameter Model, Substructure approach, Macro-element, Soil nonlinearity, Multiple-stripe analysis.

ISSN:2623-3347 © 2019 The Authors. Published by Eccomas Proceedia.
Peer-review under responsibility of the organizing committee of COMPDYN 2019.
doi: 10.7712/120119.7045.19132

1 INTRODUCTION

Recent earthquake occurrence in the northern Netherlands has been attributed to gas production activity in the Groningen field, the largest of which to date has been the Huizinge event of August 2012 with a magnitude ML 3.59 (Mw 3.53: Dost et al., 2018) [1]. In response to this induced seismicity, the operators of the field, NAM - Nederlandse Aardolie Maatschappij B.V., have been developing a comprehensive seismic hazard and risk model for the region, which comprises the entire gas field plus a 5 km buffer zone onshore (van Elk et al., 2019) [2].

A key component of the risk assessment involves the definition of fragility functions (which describe the probability of exceeding a given damage or collapse state, conditional on the intensity of input ground motion), for each building type that has been identified within the region, and included in the exposure model. At least one real representative building from the region was found for each building type (the so-called index building) and the structural drawings were used to develop a multi-degree-of-freedom (MDOF) numerical model of the structural system including the predominant non-structural elements (such as partition and external façade walls). However, the computational effort associated with running nonlinear dynamic analyses of many such numerical models, each subjected to tens or hundreds of records, was judged to be too high to allow fragility functions to be directly developed from these analyses. Therefore, a simplified single-degree-of-freedom (SDOF) equivalent system approach was used instead to analytically represent the structural system of each typology. Dynamic soil-structure interaction (SSI) is modelled through three different approaches: one-dimensional frequency-independent spring and dashpot, Lumped-Parameter Model (LPM) accounting for frequency dependence of the impedance, and using a nonlinear macro-element.

This paper investigates the impact of adopting the different SSI models listed above on the collapse fragility functions for the unreinforced masonry (URM) building types, which make up at least 85% of the building stock in the Groningen region.

2 INVESTIGATED INDEX BUILDINGS

Seven different index buildings (Arup, 2017) [3], all typically constructed with shallow foundations, have been considered herein, with the characteristics summarised in Table 1. These residential buildings are either detached or terraced (with units varying from 2 to 8) and, depending on their age, they are constructed with timber or concrete floors, and solid or cavity URM walls.

Index Building Name	System type	Floor type	Wall type	Number of storeys	Mass (tonnes)	Period (s)
Zijlvest	Terraced	Concrete	Cavity	2 + attic	219	0.34
Julianalaan	Terraced	Concrete	Cavity	2 + attic	252	0.15
E45	Terraced	Concrete	Cavity	2 + attic	315	0.24
Patrimoniumstraat	Terraced	Timber	Cavity	2 + attic	148	0.10
Kwelder	Detached	Concrete	Cavity	1 + attic	96	0.08
Badweg	Detached	Timber	Cavity	1 + attic	44	0.13
LNEC-BUILD3	Detached	Timber	Solid	1 + attic	44	0.08

Table 1: Summary of the URM index buildings with shallow foundations.

In all SSI models considered in this work, the superstructure is represented in a simplified way as a SDOF system, whose behaviour is described with the *multi_lin* material in Seismo-

Struct (Seismosoft, 2019) [4]. In order to calibrate this hysteretic model, fixed-base MDOF models for each index building were produced in LS-DYNA (LSTC, 2013) [5] and were subjected to nonlinear dynamic analysis using 11 training records (see Arup, 2017 for further details) [6]. The maximum attic displacement of a given MDOF model under each training record was converted to the equivalent SDOF displacement (see Crowley et al., 2017) [7] and then compared with the displacement obtained under the same records for the fixed-base SDOF model in SeismoStruct. The logarithms of these displacements were plotted against the logarithm of the average spectral acceleration (AvgSa) of each record, defined as the geometric mean of spectral accelerations from 0.01 to 1 second, and the linear regressions of each model compared. Afterwards, the SDOF model was iteratively adapted until a reasonable match was obtained (see Figure 1).

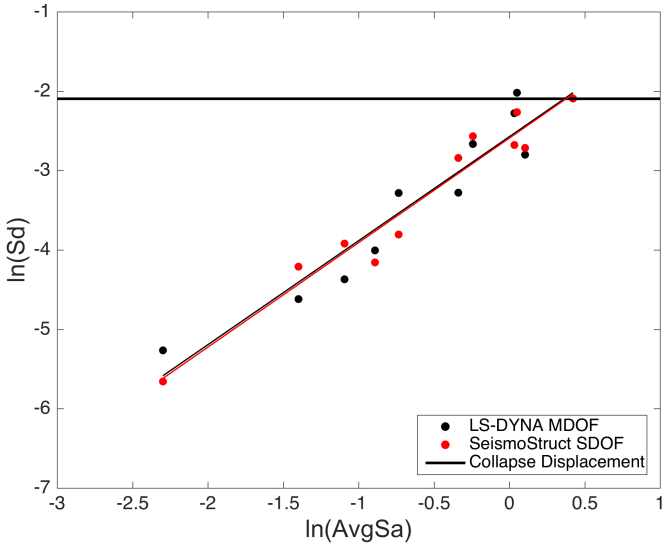

Figure 1: Comparison of displacements from MDOF (transformed to SDOF) LS-DYNA model and SDOF SeismoStruct model with calibrated *multi_lin* hysteretic model.

3 SOIL CHARACTERISATION IN GRONINGEN

In order to account for SSI it is first required to define representative soil profiles that may be used for assessment of the input parameters of the different models used (one-dimensional frequency-independent, LPM, macro-element). The selection of representative soil profiles takes advantage of the detailed microzonation carried out in recent years for the Groningen region, resulting among others in maps of the site response Amplification Factor (AF) for several spectral ordinates (Rodriguez-Marek et al., 2017) [8]. The examination of AF distributions shows that in general the patterns of high and low AF are well reflected by the geological zonation model (Bommer et al., 2017) [9]. Therefore, the AF represents well the soil behaviour of the shallow deposits, and it can be considered a reliable parameter for the identification of representative soil profiles.

The site response analysis study (carried out for ten levels of input motion) was performed for a grid of about 140’000 points homogeneously distributed in the Groningen area. Figure 2a) shows the distribution of AFs for the highest input motion level at spectral ordinates at 0.5s. Due to the non-negative values of the AF, it was assumed that AF follows a lognormal distribution.

A representative shear wave velocity profile was evaluated as the mean of *Vs* profiles around the median AF (equal to 2.25) considering all sites with AFs in an interval of amplitude equal to 0.2. The AFs corresponding to the largest input motion level were considered.

Different levels of AF and/or input motion can be selected to define alternative V_S profiles in future steps, being the median AF the most representative. The V_S profile is not the only relevant parameter for SSI, therefore a real stratigraphy, with the related parameters (strength, stiffness, etc.), needs to be identified. The simplest way to perform this operation is to identify a real stratigraphy (i.e., one of the about 140k sites considered for site response analyses) compatible with the computed mean *Vs* profile. This has been done evaluating the deviation between the mean *Vs* profile and one of the *Vs* profiles in the interval of median AF considered. Figure 2b) shows the comparison between the mean V_S profile and the V_S profile with minimum deviation.

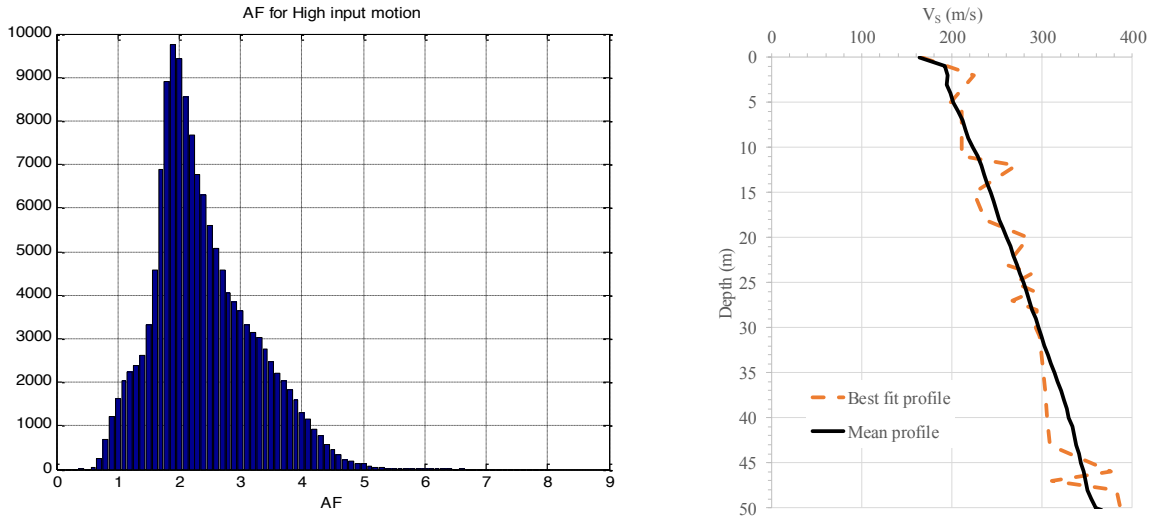

a) b)

Figure 2: a) Histogram of AF for period equal to 0.5s and high input motion; b) Mean shear wave velocity profile around median AF *vs* best fit profile. Plots were derived using data described in Kruiver et al. (2017) [10] and Rodriguez-Marek et al. (2017) [8].

The upper 30 m of the identified deposit is constituted by an alternation of fine sand and cohesive layers (i.e., clayey sand and sandy clay). In the shallow part, which mostly affects the response of shallow foundations, there is a 5 m thick layer of fine sand. The shallow water table level requires that the computation of bearing capacity be performed under undrained conditions.

In the framework of site response analysis, several soil parameters were associated to each site. Besides the V_S profile and soil stratigraphy, other geotechnical parameters used for site response analysis are included, in particular a set of geomechanical parameters used to describe the dynamic soil behaviour such as the modulus reduction and damping curves (see Kruiver et al., 2017 [10] and Rodriguez-Marek et al., 2017 [8]). Unfortunately, for fine sand, strength parameters are not available; consequently, they were defined based on existing literature, trying to constrain the selected values based on available information (i.e., V_S profile, coefficient of uniformity and D_{50}, diameter of the particle with 50% of passage in the grain size distribution). In particular, Fear and Robertson (1995) [11] proposed a framework for estimating the ultimate undrained steady state shear strength of sand (S_u) from in situ tests; the formulation combines the theory of critical state soil mechanics with shear wave velocity measurement. Figure 3 shows the undrained shear strength profile in the shallow part of the selected representative soil profile. Undrained shear strength is used to compute the bearing capacity under undrained conditions.

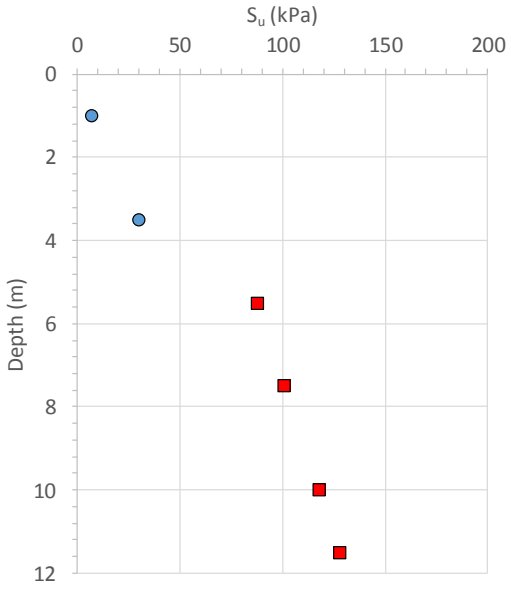

Figure 3: Undrained shear strength in the shallow part of the representative soil profile: blue circle fine sand layer, red square cohesive layer.

4 SUBSTRUCTURE APPROACH

In this work, SSI was initially analysed by the substructure approach, which allows splitting kinematic and inertial interaction in different sub-steps and considering their combined effects using the principle of superposition (Mylonakis et al., 2006) [12].

Kinematic interaction causes a modification of the free-field motion due to the geometry and stiffness of the foundation, on which a different motion is applied, called Foundation Input Motion (FIM). In practical applications, structural engineers commonly neglect the effects of kinematic interaction (Dezi et al., 2010) [13]. Arup (2015a, 2015b) [14], [15] also determined kinematic interaction to be negligible in the response of the simplified models used for definition of fragility curves. As a consequence, the free-field motion was used as input motion for the nonlinear dynamic analyses in this study.

Inertial interaction includes the dynamic response of the coupled soil-foundation-structure system due to the input motion and is characterised predominantly by a shift of structural frequencies to lower soil-structure frequencies and by an increase of damping. Within the coupled system, the soil is replaced by a set of springs and dashpots (as well as masses, in some cases) at the foundation level, representing the foundation dynamic impedance (see section 4.1). The latter is a complex-valued frequency function, whose real and imaginary parts depend on the stiffness and on the energy dissipation properties, respectively.

Two different models following the substructure approach were implemented in SeismoStruct for derivation of fragility functions. They are briefly described in sections 4.2 and 4.3.

4.1 Definition of impedance functions

Impedance functions were evaluated using the software DYNA6.1 (GRC, 2015) [16]. The foundations of the buildings considered consist of a grid of continuous beams oriented in two orthogonal directions. Conversely, the structural model used for definition of the fragility curves is a SDOF system in which the contact with the soil is limited to a single point. The geometry of grid foundations does not allow a simple and unique definition of equivalent dimensions for impedance function calculation; in fact, depending on the degree of freedom an-

alysed (i.e., translational or rotational) or on the component under consideration (i.e., stiffness or damping), the characteristics of the real foundation to be preserved are different (contact area, inertia, etc.). For such reason, in order to properly consider the real foundation geometry, the definition of the equivalent footing dimensions for impedance calculation made use of the calibration step carried out for the macro-element (see sections 5.1 and 5.2), which employs a 3D MDOF model of the buildings. For each building, equivalent dimensions were evaluated independently for stiffness and damping, as well as for the translational and rotational degrees of freedom, in order to reproduce the static stiffness and damping evaluated for the equivalent macro-element of the SDOF system described in section 5.2.

The impedance functions (i.e., stiffness and damping constants) were computed considering a composite medium (i.e., soil layer with limited depth on top of a half-space), characterised by a linear shear wave velocity profile in the upper soil layer and constant value on the half space. The layer properties (e.g., thickness, shear wave velocity) were defined taking into account the software limitations, which considers fixed values of the ratio of layer thickness to the half-width of the equivalent square footing. Moreover, the fitting of the shear wave velocity profile was carried out for a ratio between the shear wave velocity at the base of the footing and at the half-space equal to 0.6. Figure 4a) shows an example of shear wave velocity profile fitting. Given the different equivalent dimensions considered, the V_S profile fitting needs to be repeated for each of the four cases accounted for.

The software considers fixed values of material damping, equal to 0.03 for the upper layer and 0.05 for the half-space. Impedance functions were calculated considering a Poisson's ratio equal to 0.45.

Based on the results of site response analysis, scaling factors for the V_S profile were defined to account for soil nonlinearity depending on the strain level. A relationship between PGA and V_S scaling factors was obtained considering at different PGA the mean strain level and shear modulus degradation in the fine sand layer, which is characterised by two different degradation curves. Figure 4b) shows the G/G_{max} scaling factors for the two shear modulus degradation curves considered for the fine sand layer. Five PGA levels ranging from 0.05 g to 0.43 g were considered in the derivation of impedance functions.

Figure 7 shows an example of impedance functions computed using the input data described in this section.

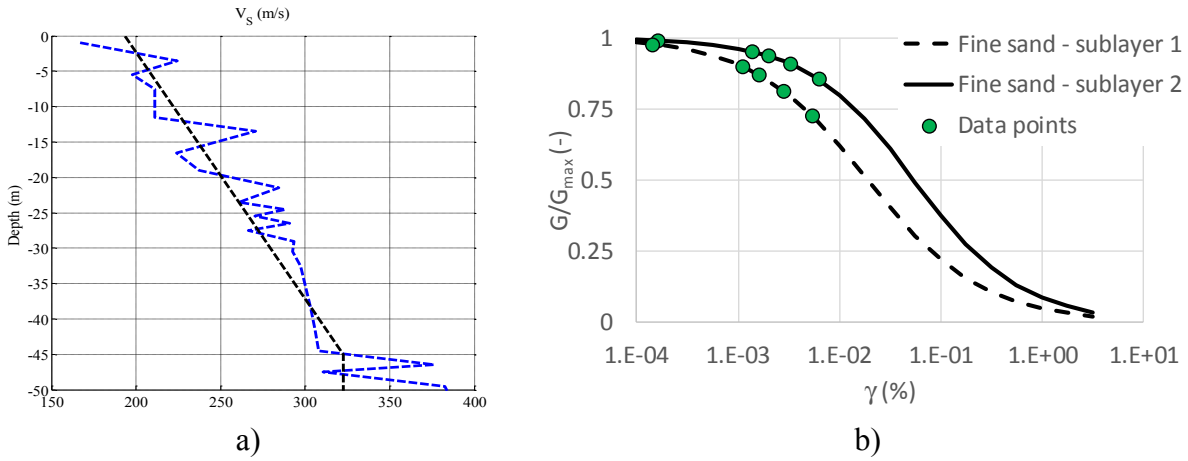

Figure 4: a) Example of shear wave velocity profile fitting; b) G/G_{max} scaling factors obtained from site response analysis for different levels of shear strain in the fine sand layer characterised by two shear modulus degradation curves.

4.2 One-dimensional frequency-independent model

The simplest SSI model employed in the fragility functions' development in this work is a one-dimensional frequency-independent model, having a lateral spring with stiffness k_x and a dashpot with viscous damping coefficient c_x. The values of the stiffness and viscous damping coefficient were obtained using the fundamental frequency of the fixed-base SDOF model together with the impedance functions derived for the Groningen field. The structural SDOF mass, stiffness and damping coefficient are indicated with m_s, k_s and c_s, respectively, in Figure 5. The seismic excitation is input to the system as an acceleration time history, $a(t)$, applied to the fixed support at the base.

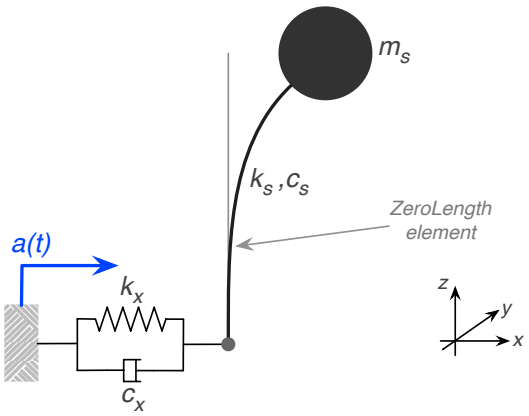

Figure 5: The adopted one-dimensional frequency-independent model.

4.3 Lumped-Parameter Model (LPM)

A Lumped-Parameter Model (LPM) accounting for frequency dependence of the impedance functions was also implemented in SeismoStruct and used for the derivation of fragility functions.

Even though techniques are available to describe frequency dependence of any type through a generalized LPM whose form is not known in advance (Lesgidis et al., 2015) [17], this work adopted the simplest LPM capable of describing approximately, over the frequency range of interest, the features of two components of impedance, namely the translational and rotational terms.

The LPM model proposed by the RINTC Workgroup (2018) [18], which is an extension of the model by Dezi et al. (2009) [19] and Carbonari et al. (2011, 2012, 2018) [20], [21], [22], was taken as a reference. Such model was simplified in order to neglect the rocking-sway coupling, because the focus in this paper is on shallow foundations. The adopted system is shown in Figure 6.

The crucial feature of this LPM is the introduction of a translational fictitious (non-physical) mass m_x in the interface node (representing the foundation), linked to the ground by a translational spring (of constant k_x) and by a dashpot (of constant c_x). This system is characterised by a frequency-dependent response to an input and thus allows for an approximate description of the frequency dependence of the impedance. Expressing the equation of motion of the system without the superstructure in the frequency domain, it can be easily seen that the dynamic impedance decreases parabolically ($k_x - m_x \omega^2$) with frequency, whereas the imaginary part increases linearly ($c_x \omega$) with frequency. In case the foundation mass is taken into account, it is added to the fictitious mass in the same node.

In order to model the foundation rotation, the LPM includes a rotational mass m_{ry} in the interface node, linked to the ground by a rotational spring (of constant k_{ry}) and dashpot (of constant c_{ry}).

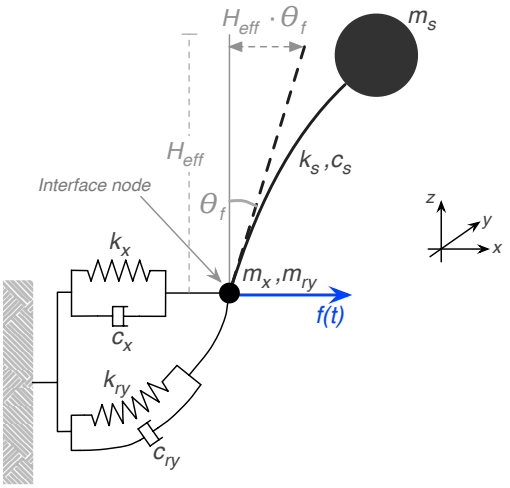

Figure 6: The adopted Lumped-Parameter Model.

The soil portion of the LPM is thus characterised by two independent degrees of freedom. The mass matrix takes the form:

$$\mathbf{M} = \begin{bmatrix} M_{11} & M_{12} \\ M_{12} & M_{22} \end{bmatrix} = \begin{bmatrix} m_x & 0 \\ 0 & m_{ry} \end{bmatrix} \tag{1}$$

The stiffness and damping matrices, **K** and **C**, are written similarly. The six diagonal terms of the matrices, namely M_{11}, M_{22}, K_{11}, K_{22}, C_{11}, C_{22}, which are coincident with the parameters of the soil portion of the LPM, are obtained by fitting two components of impedance (i.e., translational and rotational) with parabolic and linear functions for the real and imaginary parts, respectively.

Figure 7 shows an example of such fit, for a structural SDOF with first natural frequency of 7.6 Hz. In order to capture the inertial interaction effects between the superstructure and the foundation, the superstructure mass is placed above the ground at the building centroid height, H_{eff}, and is connected to the interface node by a rigid link. In this way, the rigid displacement of the superstructure mass due to the foundation rotation θ_f, and equal to $H_{eff} \cdot \theta_f$, is taken into account within the nonlinear dynamic analyses, and then subtracted from the total displacement.

The seismic excitation must be input to the LPM as a force history applied to the interface node, written as follows:

$$f(t) = m_x \cdot \ddot{u}_g + c_x \cdot \dot{u}_g + k_x \cdot u_g \tag{2}$$

in which the subscript g indicates the ground motion. This force, if applied to the interface node without the presence of the superstructure, reproduces the free-field ground excitation.

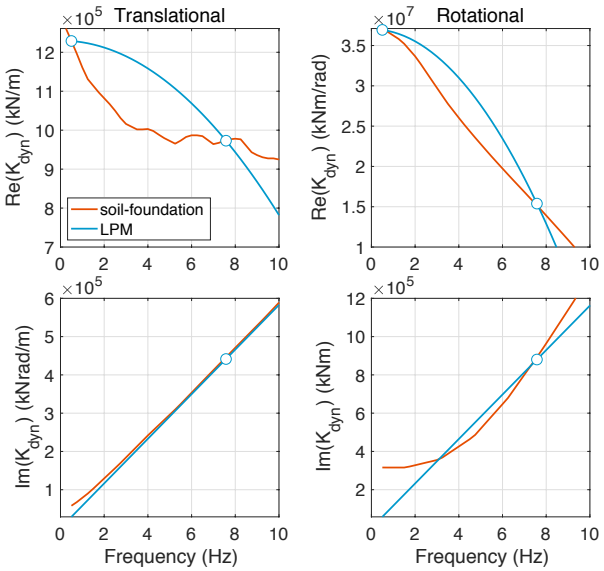

Figure 7: Sample fit of real and imaginary parts of two impedance components, in the 0 - 10 Hz frequency range.

5 HYBRID APPROACH WITH NONLINEAR MACRO-ELEMENT

Inertial interaction in presence of nonlinear soil response can be simulated through the use of soil-foundation macro-elements. The concept of macro-element has been developed by the earthquake engineering community for SSI analysis during the last 20 years. Nowadays it is frequently adopted in research studies for the reliable estimation of soil displacements, despite the complex and highly nonlinear behaviour of the foundation soil and the difficulty in assessing SSI effects (Correia, 2011, 2013) [23], [24].

In fact, macro-element models for shallow foundations have previously shown to be a cost-effective and reliable tool for such type of analysis, since they suitably represent both the nonlinear soil behaviour at the near-field and the ground substratum dynamic characteristics at the far-field, as well as the interaction with the seismic response of the structure. Hence, all aspects of elastic and inelastic behaviour of the foundation system are encompassed into one computational entity and are described by the behaviour of a single point at the centre of the foundation. Their application to seismic design is straightforward, leading to a more efficient design and to higher confidence in the predicted structural response.

The macro-element model by Correia and Paolucci (2019) [25] builds upon the innovative concepts and formulations of the models by Chatzigogos et al. (2011) [26] and by Figini et al. (2012) [27]. Nevertheless, it incorporates relevant improvements, namely addressing inconsistencies regarding the formulation of the participating mechanisms and extending their scope to three-dimensional loading cases. Moreover, this macro-element introduces an enhanced uplift model, based on a nonlinear elastic-uplift response that also considers some degradation of the contact at the soil/footing interface due to irrecoverable changes in its geometry. An improved bounding surface plasticity model and return mapping algorithms were also adopted in order to reproduce a more general and realistic behaviour, which correctly takes into account the simultaneous elastic-uplift and plastic nonlinear responses. It was implemented in SeismoStruct [4] and used herein for the derivation of fragility functions.

Following the parametric study by Pianese (2018) [28], the five calibration parameters of the macro-element became well-constrained, allowing for the dynamic response to be obtained with high confidence. The remaining parameters correspond to: (i) the footing dimensions; (ii) the six initial elastic frequency-independent values of the diagonal impedance

matrix, which can be easily obtained from literature, and which represent the far-field response; (iii) the six bearing capacity values, which can be derived from classical formulae, and which represent the near-field failure conditions. In between these two extreme types of response, the macro-element gradually evolves from the initial elastic response to the plastic flow at failure through the bounding surface plasticity model, incorporating the uplift and contact degradation phenomena.

The adopted system for nonlinear dynamic analyses, as modelled in SeismoStruct, composed of a nonlinear structural SDOF and a footing macro-element, is shown in Figure 8. As done for the LPM, in order to capture the inertial interaction between the superstructure and the foundation (with mass m_f), the superstructure mass is placed above the ground at the building centroid height, H_{eff}. The seismic acceleration, $a(t)$, is actually input to the system as an inertia force history, $f(t)$, applied to the superstructure mass: this approach properly considers the inertial components in the presence of the structure (structure and foundation masses and their interaction) and could also have been applied to the previous models, resulting in a response in terms of relative displacements with respect to the ground motion. The three springs and dashpots represented in the 2D view of Figure 8 model the macro-element elastic behaviour in the far-field. Their constants correspond to the stiffness and damping in the vertical direction (k_V, c_V), horizontal x-direction (k_{Hx}, c_{Hx}) and rotational direction around the y-axis (k_{My}, c_{My}). For simplicity, the remaining three springs and dashpots are not visualised in the 2D scheme: however, such elements are present in the macro-element implementation and play an active role in the dynamic analyses, being the macro-element behaviour fully coupled in the six directions.

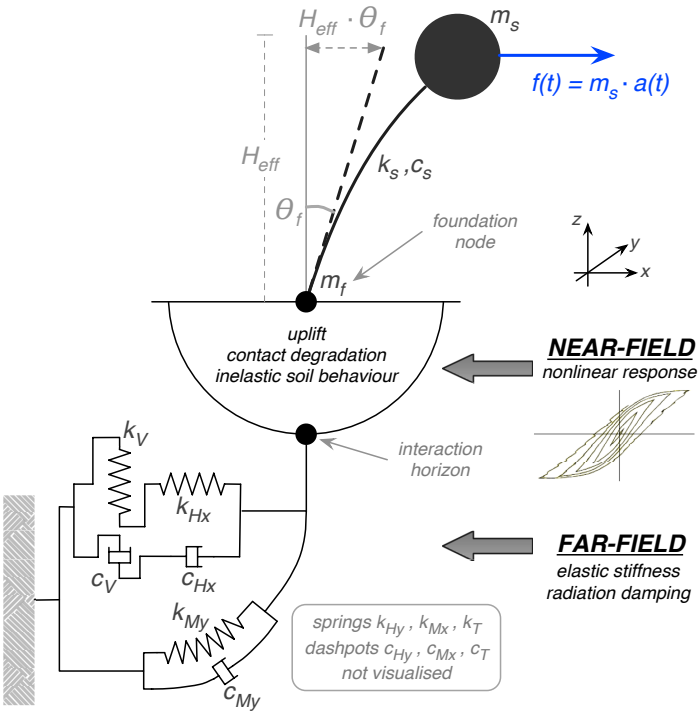

Figure 8: The adopted system with footing macro-element (shallow foundations).

Since the structural model used for the computation of fragility curves is a SDOF model, the definition of the input parameters for a representative macro-element requires a calibration step. Such calibration was carried out in order to define the characteristics of the macro-element equivalent to the real foundation system, which are composed of a grid of foundation

beams. The calibration step, described in section 5.2, was carried out considering a MDOF model for each building, in which each foundation beam was represented by a macro-element, whose characteristics were defined as described in section 5.1.

5.1 Properties of the macro-element under a single foundation beam

The input parameters of the macro-element include the foundation impedances and bearing capacity of the foundation. The derivation of both sets of information was based on the representative soil stratigraphy defined in Section 3.

The bearing capacity of the foundations was evaluated under undrained conditions, considering the undrained shear strength profile shown in Figure 3, and using the formulation proposed by EC7 (CEN, 2004) [29].

The impedance of the foundations was determined using the relationships proposed by Gazetas (1991) [30], considering rectangular foundations on homogenous half-space. As mentioned above, the macro-element requires as input constant stiffness and damping coefficients for the six degrees of freedom, which were evaluated at a frequency equal to 1.67 Hz.

5.2 Properties of the equivalent macro-element

The employed footing macro-element models the soil under a single footing or foundation beam. However, since a simplified SDOF system approach was used to represent the structural system, the derivation of an "equivalent" macro-element for an entire building was needed.

To this end, the first step was to build a MDOF model for each index building. Figure 9 shows the models built in SeismoStruct for both terraced and detached buildings.

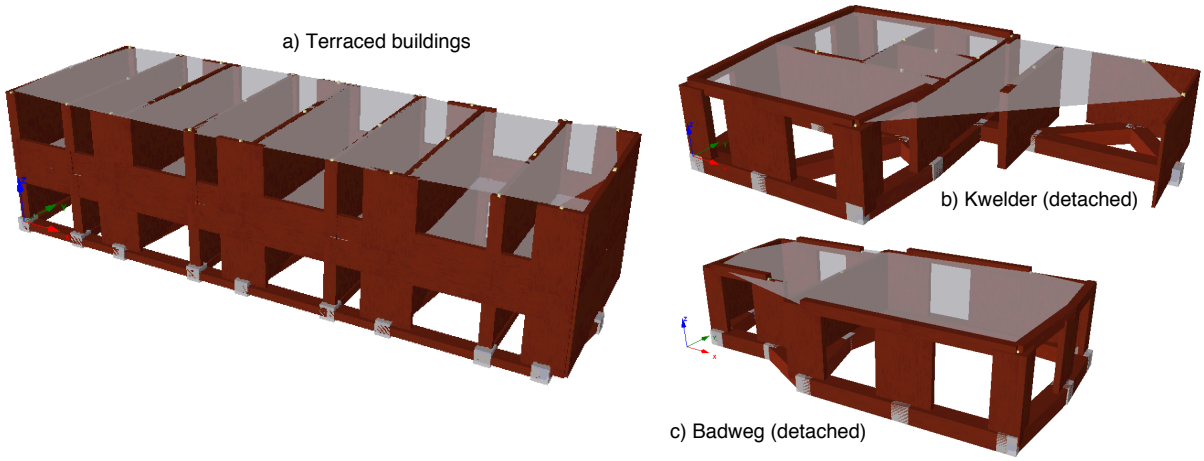

Figure 9: MDOF models in SeismoStruct for the investigated index buildings.

Given the similarity of geometric properties for all the considered terraced index buildings, the same model (Figure 9a) was used for all of them, only changing the total mass accordingly. For the same reason, the model for Badweg (Figure 9c) was used also for the shake table test specimen LNEC-BUILD3. Masonry piers and spandrels were introduced as columns and beams, respectively. The rigid reinforced concrete slabs were modelled with rigid diaphragms linking the column nodes at the floor levels. The total number of footing macro-elements included at the base of the models, in correspondence to the centroid of masonry piers, is 27 for terraced buildings, 16 for Kwelder, and 13 for Badweg. Reinforced concrete foundation beams connect the upper nodes of the macro-elements. Both masonry and reinforced concrete were considered as linear elastic materials, in the MDOF models, with the actual values for

the elastic modulus and density. The total masses of the models, given by the superstructure mass plus the foundation mass, are approximately equal to the actual total masses, which were used in the derivation of the single macro-element properties as described in Section 5.1.

The equivalent macro-element calibration requires the computation of the (elastic) stiffnesses, bearing capacity and damping coefficients along the six directions. Most of the parameters were computed analytically starting from the foundation geometry and properties of the single macro-elements, while the remaining ones required the output from the model. The model output parameters needed for the calibration are the vertical reactions of the macro-elements and the base shear capacities in the two horizontal directions x and y: both output results were obtained from two pushover analyses, along x and y. The latter were carried out pushing the structure in load control with point forces located at the floor levels, according to a triangular distribution.

The vertical stiffness, k_V, torsional stiffness, k_T, as well as the horizontal stiffness in the two directions, k_{Hx} and k_{Hy}, were obtained by simply summing up the stiffness values of the single macro-elements, assuming a rigid behaviour of the foundation plane. For the rotational stiffness in the two directions, k_{Mx} and k_{My}, the lower bound would be simply the sum over the single macro-elements, as done for the other stiffness components, while adopting the upper bound would mean accounting for both the rotational stiffness of each macro-element and their vertical stiffness contribution for a rigid rotation of the foundation plane. For the case at hand, it was decided to employ the rotational stiffness upper bound, consistently with the rigid foundation plane assumption adopted for the horizontal stiffness. Since the dynamic behaviour of buildings on shallow foundations is driven more by sliding than by rocking, this choice should not lead to important variations in the results. To verify this, the fragility curves were also retrieved by using a reduced rotational stiffness, in between the two extreme values. In particular, based on expert judgement, rather than rigorous mechanical considerations, one tenth of the upper bound was adopted, a value that is of course larger than the lower bound. For all the considered buildings, this reduced stiffness led to small to negligible variations in the fragility curve with respect to the one obtained with the upper bound, as expected.

Concerning the bearing capacity, the vertical component, $N_{\max}$, was computed as the sum over the single macro-elements, while for the other components the fully coupled behaviour of the macro-element in the six directions was used for defining the size of its bounding surface. In particular, the bearing capacity in the horizontal direction, $H_{\max}$, was obtained as follows:

$$H_{\max} = \frac{\sum_{i=1}^{nME} Q_{NH,i} \cdot H_{\max,i}}{Q_{NH}} \tag{3}$$

where nME is the total number of macro-elements in the model, $H_{\max,i}$ is the maximum horizontal capacity of each macro-element in the direction considered, and Q_{NH} and $Q_{NH,i}$ are function of the applied vertical load, for the equivalent macro-element and for each of the single macro-elements, respectively. This function of the applied vertical load relates the maximum horizontal capacity of the macro-element with its actual horizontal shear capacity. Further details on the involved quantities can be found in Correia and Paolucci (2019) [25].

In order to obtain the rotational bearing capacity, $M_{\max}$, the 3D vertical-horizontal-rotational interaction surface for the capacity was used to derive the following expression:

$$M_{\max} = \frac{\sum_{k=1}^{N_s} F_{u,k} \cdot h_k}{Q_{NM}\sqrt{1-\left(\frac{H_u}{Q_{NH} \cdot H_{\max}}\right)^2}} \tag{4}$$

where $F_{u,k}$ is the ultimate horizontal force at the k-th floor level, obtained from a pushover analysis in the relevant horizontal direction and considering a triangular distribution along the building height, N_s is the number of storeys, h_k is the height of the k-th floor level, and H_u is the sum of $F_{u,k}$ for all storeys and corresponds to the ultimate base shear value. Q_{NH} was already defined, while Q_{NM} is also a function of the applied vertical load that relates the maximum rotational moment capacity of the macro-element with its actual moment capacity. The torsional capacity is of no interest for the 2D analyses performed.

The damping constants modelling the radiation damping in the soil along the six directions were computed by summing up the values of the single macro-elements. In what concerns the rocking response this corresponds to a lower bound assumption. Nonetheless, as mentioned above, the response of the buildings considered is mainly dominated by sliding and not by rocking.

Finally, the five calibration parameters introduced above, controlling the uplift initiation, the soil/footing contact degradation, the reference plastic modulus, the unloading/reloading parameter and the plastic potential parameter, assumed values consistent with the calibration procedure done in the work by Pianese (2018) [28]. The scallop shape was assumed for the bounding surface, since the dynamic analysis is performed under undrained conditions.

6 FRAGILITY FUNCTIONS

This section briefly describes the methodology proposed in this work to derive the collapse fragility functions for the investigated index buildings, and then compares the curves obtained through the different approaches.

6.1 Methodology

Hazard-compatible records for the development of fragility functions were selected through disaggregation of seismic hazard at four different return periods (500, 2500, 10k and 100k years) at one of the highest hazard locations in the field. Four sets of 50 spectra, conditional on four different levels (corresponding to the four return periods) of AvgSa, were determined using the mean magnitude and distance from the disaggregation together with the 2017 ground motion prediction equation for the Groningen field (Bommer et al., 2017) [9]. The records were selected from a large database, including European and NGA-West records, using the ground motion selection procedure proposed by Baker and Lee (2018) [31].

Using multiple-stripe analysis (MSA), for each of the four values of AvgSa (i.e., the stripes), the selected 50 records were used together with the SSI and SDOF models in SeismoStruct to calculate the maximum displacements. The logarithms of these displacements are plotted against the logarithm of AvgSa and then a censored linear regression is undertaken to obtain the parameters of the fragility functions (as shown in Figure 10 and described further in Crowley et al., 2017 [7]).

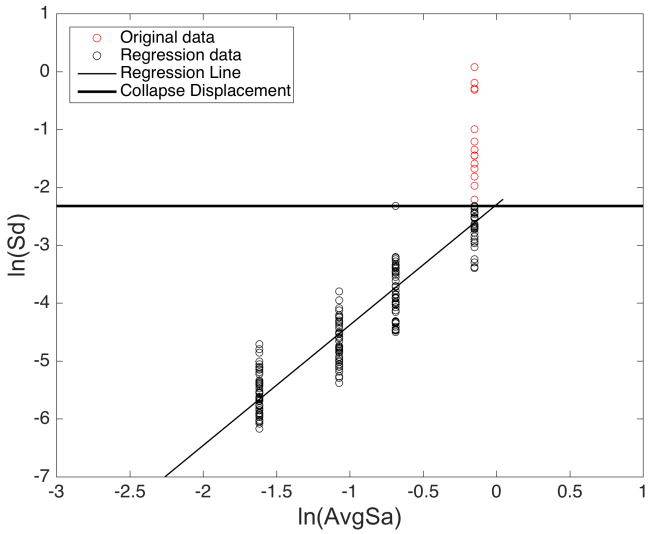

Figure 10: Example linear regression of the stripes of displacement responses of the SSI + SDOF system.

6.2 Proposed fragility functions and comparison

The obtained fragility curves for the collapse limit state and for the seven investigated index buildings are shown in Figure 11. Each subplot displays the curves related to: i) the simple one-dimensional elastic SSI case, ii) the LPM elastic SSI case, and iii) the nonlinear macro-element SSI case. The curve for the fixed-base case is also displayed for reference. It can be noted, in general, that for these buildings with shallow foundations the influence of SSI is small to negligible, and leads the curves to be shifted to the right with respect to the fixed-base case: this means that SSI may have a beneficial effect on the seismic vulnerability of these buildings.

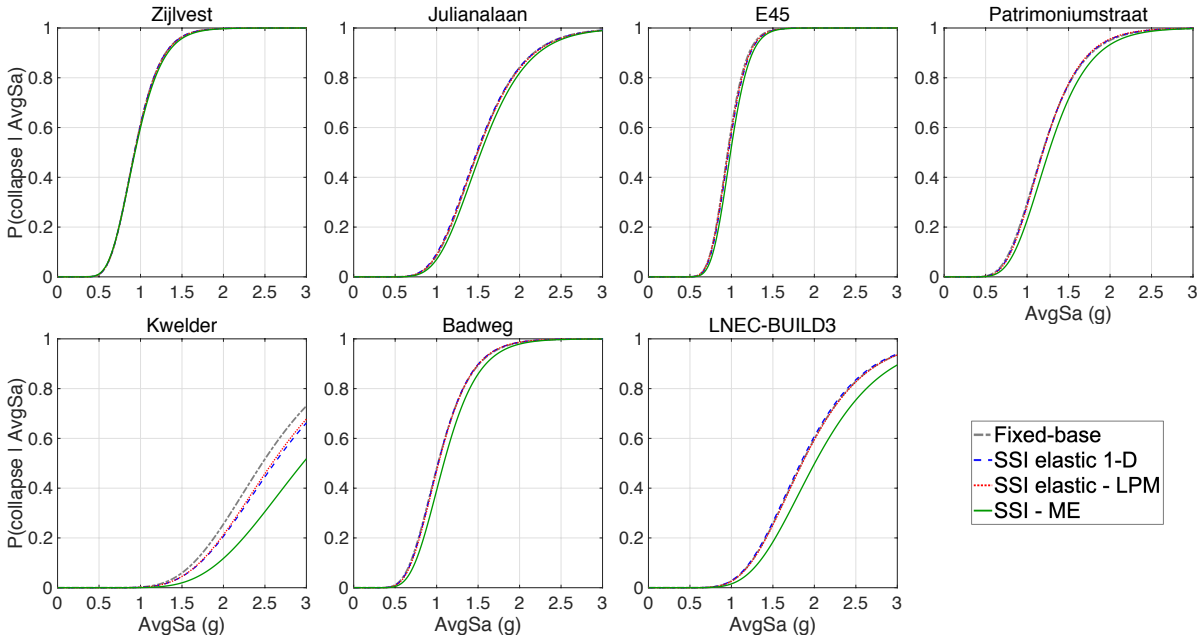

Figure 11: Proposed fragility curves for the investigated index buildings and the different SSI models.

Another remark concerns the comparison between the two elastic SSI cases and the nonlinear macro-element case. For Zijlvest the three curves coincide, while for all other buildings

the curve for macro-element is generally shifted to the right, indicating that the considered inelastic behaviour effectively leads to energy dissipation and therefore to smaller structural displacements.

Also, a quite evident difference can be noted for Kwelder and LNEC-BUILD3, in comparison to the others. Indeed, since these two buildings are much stronger and stiffer than all the others, the response of the relatively weak soil inevitably plays a more determinant role in the overall fragility of the system, and hence not only the impact of the SSI modelling becomes evident, but so does also the significance of modelling explicitly soil nonlinearity.

7 CONCLUSIONS

In recent years, the Groningen region (northern Netherlands) has been affected by induced seismicity attributed to gas production activity. Within the comprehensive seismic hazard and risk model for the region developed by NAM, the definition of fragility functions for several URM index buildings is crucial. With reference to seven of these representative buildings (considered here as SDOF systems) with shallow foundations, this paper investigated the impact of adopting alternative models of SSI on the collapse fragility functions. Two of such SSI models, namely the one-dimensional frequency-independent and the LPM, are elastic, whereas the remaining one adopts a nonlinear macro-element to encompass all aspects of elastic (in the far-field) and inelastic (in the near-field) behaviour of the foundation system.

The influence of SSI resulted to be small to negligible, and in general leads to fragility curves that are less unfavourable with respect to the fixed-base case. Moreover, the paper showed that taking into account the inelastic behaviour of the soil-foundation system may lead to smaller structural displacements and hence a lower vulnerability of the structures.

Future work aims to extend the study to buildings on piles, for investigating the influence of SSI and of the nonlinear macro-element in the presence of a different foundation system.

ACKNOWLEDGEMENTS

This work was undertaken within the framework of the research programme for hazard and risk of induced seismicity in Groningen sponsored by the Nederlandse Aardolie Maatschappij BV (NAM). In addition, the authors are also particularly grateful to Pauline Kruiver, who kindly provided access to the soil mechanical characterisation data and response analysis results for the Groningen region.

REFERENCES

[1] B. Dost, B. Edwards, J.J. Bommer, The relationship between M and M_L—a review and application to induced seismicity in the Groningen gas field, the Netherlands. *Seismological Research Letters*, **89**(3), 1062–1074, 2018.

[2] J. van Elk, S.J. Bourne, S. Oates, J. J. Bommer, R. Pinho, H. Crowley, A probabilistic model to evaluate options for mitigating induced seismic risk. *Earthquake Spectra*, *in press*, 2019.

[3] Arup, *EDB V5 Data Documentation*, Tech. Rep. 229746_052.0_REP2005, available at: http://www.nam.nl/feiten-en-cijfers/onderzoeksrapporten.html, 2017.

[4] Seismosoft, *SeismoStruct 2019 – A computer program for static and dynamic nonlinear analysis of framed structures*, available at: http://www.seismosoft.com, 2019.

[5] LSTC—Livermore Software Technology Corporation, *LS-DYNA—a general-purpose finite element program capable of simulating complex problems*. Livermore, 2013.

[6] Arup. *Typology modelling: analysis results in support of fragility functions—2017 batch results*. 229746_031.0_REP2005, NAM Platform, November 2017.

[7] H. Crowley, B. Polidoro, R. Pinho, J. van Elk, Framework for developing fragility and consequence models for local personal risk. *Earthquake Spectra*, **33**(4), 1325–1345, 2017.

[8] A. Rodriguez-Marek, P. P. Kruiver, P. Meijers , J. J. Bommer, B. Dost, J. van Elk, D. Doornhof, A Regional Site-Response Model for the Groningen Gas Field. *Bulletin of the Seismological Society of America*, **107(**5), 2067–2077, 2017.

[9] J.J. Bommer, B. Edwards, P.P. Kruiver, A. Rodriguez-Marek, P.J. Stafford, B. Dost, M. Ntinalexis, E. Ruigrok, J. Spetzler, *V5 ground-motion model for the Groningen Field*, NAM Platform, October 2017.

[10] P.P. Kruiver, E. van Dedem, R. Romijn, G. de Lange, M. Korff, J. Stafleu, J.L. Gunnink, A. Rodriguez-Marek, J.J. Bommer, J. van Elk, D. Doornhof, An integrated shear-wave velocity model for the Groningen gas field, The Netherlands. *Bulletin of Earthquake Engineering*, **15**(9), 3555–3580, 2017.

[11] C.E. Fear, P.K. Robertson, Estimating the undrained strength of sand: a theoretical framework. *Canadian Geotechnical Journal*, **32**, 859-870, 1995.

[12] G. Mylonakis, S. Nikolaou, G. Gazetas, Footings under seismic loading: Analysis and design issues with emphasis on bridge foundations. *Soil Dynamics and Earthquake Engineering*, **26**(9), 824-853, 2006.

[13] F. Dezi, S. Carbonari, G. Leoni, Kinematic bending moments in pile foundations. *Soil Dynamics and Earthquake Engineering*, **30**(3), 119-132, 2010.

[14] Arup, *Soil-Structure Interaction for Linear Analysis - Groningen Earthquakes - Structural Upgrading*. Report N. 229746_032.0_REP102. Issue Rev.0.04 | 16 February 2015.

[15] Arup, *Soil-Structure Interaction for Nonlinear Static Analysis - Groningen Earthquakes - Structural Upgrading*. Report N. 229746_032.0_REP118. Issue Rev.0.02 | 27 February 2015.

[16] GRC - Geotechnical Research Centre of Western Ontario University, *DYNA6.1 – A program for the computation of the response of rigid foundations to all types of dynamic loads*. Ontario, Canada, 2015.

[17] N. Lesgidis, O.S. Kwon, A. Sextos, A time-domain seismic SSI analysis method for inelastic bridge structures through the use of a frequency-dependent lumped parameter model. *Earthquake Engineering & Structural Dynamics*, **44**(13), 2137-2156, 2015.

[18] RINTC Workgroup, *Results of the 2015-2017 Implicit seismic risk of code-conforming structures in Italy (RINTC) project*. ReLUIS report, Rete dei Laboratori Universitari di Ingegneria Sismica (ReLUIS), Naples, Italy, available at http://www.reluis.it/, 2018.

[19] F. Dezi, S. Carbonari, G. Leoni, A model for the 3D kinematic interaction analysis of pile groups in layered soils. *Earthquake Engineering & Structural Dynamics*, **38**(11), 1281-1305, 2009.

[20] S. Carbonari, F. Dezi, G. Leoni, Linear soil–structure interaction of coupled wall–frame structures on pile foundations. *Soil Dynamics and Earthquake Engineering*, **31**(9), 1296-1309, 2011.

[21] S. Carbonari, F. Dezi, G. Leoni, Nonlinear seismic behaviour of wall-frame dual systems accounting for soil-structure interaction. *Earthquake Engineering & Structural Dynamics*, **41**(12), 1651-1672, 2012.

[22] S. Carbonari, M. Morici, F. Dezi, G. Leoni, A lumped parameter model for time-domain inertial soil-structure interaction analysis of structures on pile foundations. *Earthquake Engineering & Structural Dynamics*, **47**(11), 2147-2171, 2018.

[23] A.A. Correia, *A pile-head macro-element approach to seismic design of monoshaft-supported bridges*, Ph. D. thesis, European School for Advanced Studies in Reduction of Seismic Risk, (ROSE School), Pavia, Italy, 2011.

[24] A.A. Correia, Recent advances on macro-element modeling: shallow and deep foundations. Proceedings of *Final workshop of project Compatible soil and structure yielding to improve system performance (CoSSY)*, Oakland, USA, 2013.

[25] A.A. Correia, R. Paolucci, A 3D coupled nonlinear shallow foundation macro-element for seismic soil-structure interaction analysis (in preparation), 2019.

[26] C.T. Chatzigogos, R. Figini, A. Pecker, J. Salençon, A macroelement formulation for shallow foundations on cohesive and frictional soils. *International Journal for Numerical and Analytical Methods in Geomechanics*, **35**(8), 902-931, 2011.

[27] R. Figini, R. Paolucci, C.T. Chatzigogos, A macro-element model for non-linear soil-shallow foundation-structure interaction under seismic loads: theoretical development and experimental validation on large scale tests. *Earthquake Engineering and Structural Dynamics*, **41**(3), 475-493, 2012.

[28] G. Pianese, *Non-linear effects on the seismic response of buildings with foundation-structure interaction*, Ph. D. thesis, Politecnico di Milano, Milan, Italy, 2018.

[29] CEN - Comité Européen de Normalisation, *Eurocode 7: Geotechnical design - Part 1: General rules*, ENV 1997:1-1994, 2004.

[30] G. Gazetas, *Foundation vibrations*, in *Foundations Engineering Handbook*, *2nd edition*, Fang H.Y. (Editor), New York, Van Nostrand Reinholds, pp. 553–593, chapter 15, 1991.

[31] J.W. Baker, C. Lee, An improved algorithm for selecting ground motions to match a conditional spectrum. *Journal of Earthquake Engineering*, **22**(4), 708-723, 2018.